Recombination-Generation and Optical Properties of Gold Acceptor in Silicon*

A. F. TASCH, JR.,† AND C. T. SAH
Departments of Electrical Engineering and of Physics and Materials Research Laboratory, University of Illinois, Urbana, Illinois 61801

(Received 11 August 1969)

The thermal emission rates of electrons and holes at the gold acceptor center ($E_C - E_{Au-} = 540$ meV) in silicon are obtained from 200 to 300°K in silicon using the photovoltaic effect in the depletion region of a reverse biased p-n junction. The observed electric field dependences are considerably smaller than that predicted by the three-dimensional Poole-Frenkel effect in a Coulombic potential, but closer to that in a polarization potential. The ratio $e_n{}^t/e_p{}^t$ is 50 at 190°K and decreases to 16 at 300°K. The low field values of the thermal emission rates, $e_n{}^t$ and $e_p{}^t$, are used to compute the thermal-capture cross sections of electrons and holes which show $\sigma_n{}^t \propto T^0$ and $\sigma_p{}^t \propto T^{-4}$ and are consistent with Lax's impurity model. The degeneracy factors obtained from these emission-rate data and the capture-cross-section data of Fairfield and Gokhale are 15 and 7.5 for the electron and hole transitions, which are not inconsistent with those of the one-band model. The photoionization cross sections of electrons and holes and their spectral dependences are also obtained from -56 to -78°C and compared with the δ-function impurity potential model of Lucovsky, giving an effective-field ratio of $(m/m^*)^{\frac{1}{2}}(\epsilon_{eff}/\epsilon_0) \sim 3$–$4$ for holes and ~ 1.3 for electrons. No temperature and field dependences are observed. Radiative recombination cross sections obtained from detailed balance are 6.3×10^{-21} cm² for holes and 3×10^{-21} cm² for electrons at 300°K.

I. INTRODUCTION

THE recombination-generation and optical properties of impurity centers in semiconductors are characterized by the bound-state energy levels within the energy gap, the thermal-capture cross sections, the thermal emission or ionization rates, and the photoionization cross sections of electrons and holes. The majority of the investigations on the recombination-generation properties give the carrier-capture cross sections from various methods of lifetime measurements of excess carriers. Many of these methods encounter some difficulties in measurement technique and interpretation of data due to the very fast recombination decay time, the appearance of two or more time constants and frequently distributed time constants with nonexponential decay, and the considerable inaccuracy in measuring the important parameters such as the impurity and carrier concentrations.

In this paper, the recently proposed new method based on the impurity photovoltaic effect,[1,2] which is free from all of these uncertainties, is applied to a detailed study of the gold acceptor centers in silicon. Here, the carrier-generation kinetics, rather than the recombination kinetics in the classical photoconductivity decay method, is observed. The experimental photocurrent waveform provides directly the thermal and photoionization rates of electrons and holes trapped at the impurity centers, without the necessity of knowing the impurity concentration from other measurements. The photocurrent waveforms are truly exponential and usually contain only one time constant (from microseconds to hours) which is much longer and more readily measurable than the recombination lifetime (usually nanoseconds). An analysis of the waveforms also gives the photoionization cross sections and the location of the impurity energy level. In addition, electric-field dependences of the thermal-emission rates and the photoionization cross sections can be clearly observed in this experiment and are studied.

II. THEORY

The impurity photocurrent experiments of this paper make use of reverse biased p-i-n silicon junctions ($p+n$ or $n+p$ abrupt junctions can also be used with a considerable variation of electric field across the depletion region) which is doped with gold impurity. The applied reverse-bias voltage is high enough so that the middle i region is nearly completely depleted of free carriers. Thus, thermal capture of carriers in the i region can be neglected compared with thermal and optical generations. Monochromatic chopped light above the threshold or ionization energy of trapped electrons or holes is directed onto the depleted i region to excite the electrons or holes into the conduction or valence band. The photon energy is limited to less than the gap energy so that there is no interband or intrinsic photoexcitation of electron-hole pairs whose rate is so high as to overwhelm the impurity photocurrent completely.

The short-circuit junction photocurrent due to the chopped light will now be analyzed, taking a gold-doped silicon p-i-n diode as an example. The gold impurity has an acceptor level at 0.54 eV below the conduction band edge and a donor level at 0.35 eV above the valence band edge of silicon. The donor level can be neglected if the photon energy is insufficient to photoexcite the electron trapped at a neutral gold atom to the conduction band, i.e., $\hbar\omega < E_C - E_{Au+} \simeq 0.77$ eV. The validity of this approximation is discussed in the Appendix.

* Work based in part on a Ph.D. thesis in physics of A. F. T. and supported in part by the Advanced Research Projects Agency and the U. S. Air Force Office of Scientific Research.

† Present address: Central Research Lab., Texas Instruments, Inc., Dallas, Tex. 75222.

[1] C. T. Sah and A. F. Tasch, Jr., Phys. Rev. Letters **19**, 69 (1967).
[2] C. T. Sah, A. F. Tasch, Jr., and D. K. Schroder, Phys. Rev. Letters **19**, 71 (1967).

The analyses of the current waveform of the present case and cases with different initial conditions have been given in detail elsewhere[3] based on the Shockley-Read-Hall kinetic model.[4] The rate equation of the trapped electron at the gold center, n_T, is given by[1]

$$-dn_T/dt=(c_n{}^t n+e_n{}^t+c_p{}^t p+e_p{}^t)n_T -(c_n{}^t n+e_p{}^t)N_{TT}+g_n{}^0-g_p{}^0, \quad (1)$$

where $g_n{}^0=n_T\sigma_n{}^0\Phi=n_T e_n{}^0$ and $g_p{}^0=(N_{TT}-n_T)\sigma_p{}^0\Phi=(N_{TT}-n_T)e_p{}^0$ are the optical-generation rates of electrons and holes. The c's and e's denote the capture and emission rates of electrons and holes, respectively. The superscript t denotes the phonon-aided or thermal transitions, while 0 denotes the optical transitions. $\sigma_n{}^0$ and $\sigma_p{}^0$ are the photoionization cross sections of electrons and holes, Φ is the incident monochromatic light flux, and N_{TT} is the impurity concentration of the deep-level impurity. Multiple reflection and absorption by various layers were taken care of in the data analysis and included in Φ.

The principal feature of the present method is that in the depletion region of a reverse biased p-n junction, n, $p\simeq 0$ so that the nonlinear thermal capture terms in (1) can be dropped. The resultant kinetic equation has a simple exponential solution which can then be employed to obtain the photocurrent. The result contains a steady-state term and a time-dependent term. The time-dependent term contains two components: a drift current and a displacement current, which contains the discontinuity when the light is turned on or off.[3]

The junction current density during the turn-on phase of a square wave chopped-light excitation is given by[3]

$$j_{on}(t)=-qW\tau_{on}e_n e_p N_{TT}-\tfrac{1}{2}qWN_{TT}(e_n-e_p) \times\{\tau_{off}e_p{}^t-\tau_{on}e_p\}\exp(-t/\tau_{on}), \quad (2)$$

where

$$\tau_{on}{}^{-1}=e_n+e_p\equiv e_n{}^t+e_n{}^0+e_p{}^t+e_p{}^0 \quad (3)$$

and

$$\tau_{off}{}^{-1}=e_n{}^t+e_p{}^t. \quad (4)$$

Here, $e_n=e_n{}^t+e_n{}^0$ and $e_p=e_p{}^t+e_p{}^0$ are the total emission rates of electrons and holes, respectively, including both the thermal and optical processes. W is the width of the depleted I region and is assumed to be constant during illumination. For a p-i-n junction structure, this is a good assumption.

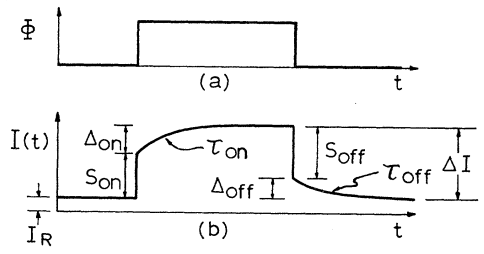

FIG. 1. (a) Square light flux and (b) photocurrent waveform with symbols used in the analyses of data discussed in Sec. II.

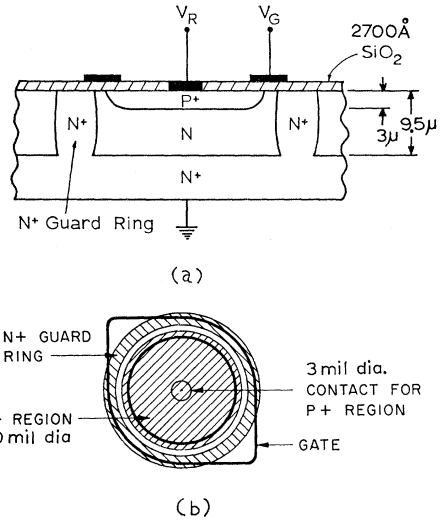

FIG. 2. Diode structure used in experiments. (a) Cross sectional view with thickness in microns; (b) top view.

When the light is turned off, the photocurrent decay is given by[3]

$$j_{off}(t)=-qW\tau_{off}e_n{}^t e_p{}^t N_{TT}-\tfrac{1}{2}qWN_{TT}(e_n{}^t-e_p{}^t) \times\{\tau_{on}e_p-\tau_{off}e_p{}^t\}\exp(-t/\tau_{off}), \quad (5)$$

which is identical to (2) if e^t and e are interchanged.

An example of the photocurrent waveform is illustrated in Fig. 1(b) for the chopped light flux shown in Fig. 1(a). The portions of the photocurrent associated with the abrupt or step rise and drop are denoted by S_{on} and S_{off}, while Δ_{on} and Δ_{off} represent those parts associated with the slower exponential rise and decay. The ratio S_{on}/S_{off} and Δ_{on}/Δ_{off} can then be written as

$$S=\frac{S_{on}}{S_{off}}=\frac{\tau_{off}}{\tau_{on}}\Big/\left(1+\frac{2e_n{}^0e_p{}^0}{e_n{}^0e_p{}^t+e_p{}^0e_n{}^t}\right) \quad (6)$$

and

$$\Delta=\Delta_{on}/\Delta_{off}=1+(e_n{}^0-e_p{}^0)/(e_n{}^t-e_p{}^t). \quad (7)$$

Thus, from (3), (4), (6), and (7) the four emission rates, $e_n{}^t$, $e_p{}^t$, $e_n{}^0$, and $e_p{}^0$, can be computed from the experimental data of τ_{on}, τ_{off}, S, and Δ. The sums $e_n{}^t+e_p{}^t$ and $e_n{}^0+e_p{}^0$ may be readily obtained from τ_{on} and τ_{off} while the differences are given by

$$e_n{}^0-e_p{}^0=\pm[(\Delta-1)(1+E)(1-S)/ E(1+E-S\Delta)]^{1/2}(e_n{}^0+e_p{}^0) \quad (8)$$

and

$$e_n{}^t-e_p{}^t=(e_n{}^0-e_p{}^0)/(\Delta-1), \quad (9)$$

where $E=(e_n{}^0+e_p{}^0)/(e_n{}^t+e_p{}^t)$. The two choices of sign

[3] C. T. Sah, L. Forbes, L. L. Rosier, and A. F. Tasch, Jr., Solid State Electron. (to be published).
[4] W. Shockley and W. T. Read, Jr., Phys. Rev. 87, 835 (1952).

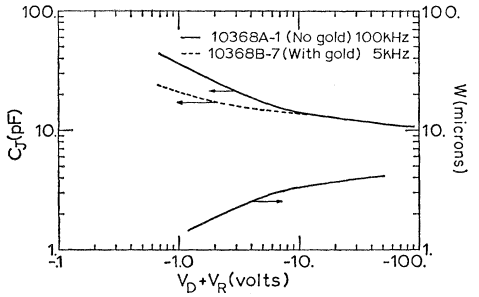

FIG. 3. Junction capacitance and depletion layer width as a function of applied reverse bias V_R and measurements signal frequency. $V_D=0.7$ V.

in (8) arise since the theory is symmetrical with respect to electrons and holes. This ambiguity can be resolved if the energy level of the impurity is appreciably closer to one of the band edges than the other. Since the gold acceptor level is located near the middle of the band gap, choice of the sign must be determined by other experiments. This point is discussed in Sec. III.

III. EXPERIMENTAL DETAILS

Gate-controlled *p-i-n* structures shown in Fig. 2(a) were fabricated for these experiments using conventional silicon transistor fabrication technology. The diodes have a doping profile of $P+NN+$ where N is a lightly doped epitaxial film grown on the $N+$ substrate, while the $P+$ region is obtained by high-temperature diffusion of boron impurity through the oxide window. The doping of the middle N region is sufficiently low so that the theory using the *p-i-n* structure may be used. The depletion region width is essentially constant and equal to the width of the N layer during illumination. The metal gate electrode shown in Fig. 2 was included to prevent surface breakdown of the junction around the curved edge of the diffused $P+$ region. Negative voltage applied to the gate will reduce the curvature, and hence the electric field, so that the avalanche breakdown voltage is raised. The ring-shaped gate electrode also shields the incident light from that part of the $P+N$ junction which intersects the SiO_2-Si interface. This optical shield then prevents optical excitation near the surface region which give complicated field dependences. The $N+$ diffused guard ring was designed to prevent the junction depletion region from extending beyond the metal gate.

The $N+$ substrate doping was 3×10^{18} donors/cm^3 while the doping in the epitaxial film was 10^{15} donors/cm^3. The diameter of the $P+$ region was 0.030 in. whose thickness and doping were such that there was negligible free-carrier absorption of the incident light. Both control (no gold added intentionally) and gold-doped devices were fabricated and mounted on *TO*-5 three-pin headers whose top view is shown in Fig. 2(b). These devices underwent identical high temperature, photoengraving and chemical etching process steps except that the gold-doped units were gold diffused at 1000°C in argon atmosphere from 99.999% purity gold layer which was evaporated onto the backside ($N+$ substrate surface) of the silicon slice.

In the experimental measurement setup, the samples were mounted on a copper block inside of a variable temperature optical Dewar and were electrically insulated from the copper block by beryllium oxide which provides good thermal contact to the copper. The sample mounting was such that the incident light was normal to the plane of the junction. The devices were shielded from all stray room light and to a large extent from the blackbody radiation from the outside Dewar wall and other parts of the apparatus whose temperatures are above that of the device. The shielding from blackbody radiation is of ultimate importance for very low level illumination or long time-constant measurements at low temperatures and for shallower level impurities whose energy level falls into the blackbody range.

The temperature of the device was measured using a platinum-resistance thermometer mounted in the copper block approximately 1 cm from the device. The thermometer is factory calibrated to better than ±0.1°C and a Honeywell model 1551-E Mueller bridge was used to measure the resistance of the thermometer. Better than ±0.05°C could be maintained during the time of recording the photocurrent waveform.

A Bausch and Lomb high-intensity grating monochromator with a 1.4–3.2-μ grating and a tungsten light source were employed. The energy spread is approximately 0.01 eV. A silicon filter was used to suppress higher orders of diffracted light from the grating in the range of 1.4 to 1.85 μ and a germanium filter was used from 1.85 to 2.2 μ. The light flux was measured by a lead sulfide detector which was calibrated against a factory-calibrated thermopile. In almost all of the measurements, the light flux was less than 250 μW/cm^2.

For temperatures below 225°K, the dark leakage current of the junction was low enough to allow photocurrent measurements directly with a Keithley 610B electrometer whose output was traced on a strip-chart recorder. Above this temperature, the short circuit photocurrent was taken off a sufficiently small-load resistor in series with the junction bias circuit. This signal was then amplified and fed into a waveform sampling and storage device to average out the noise. The output was again recorded on a strip chart recorder.

Various preliminary measurements were taken on the devices in order to obtain information about their dark current-voltage characteristics. For a sufficiently negative gate voltage, the breakdown voltage is "reach-through" limited, i.e., the depletion layer extends over the entire n region. Further increase of the reverse-bias voltage results in an increase of the electric field in the middle n region until breakdown occurs. The reach-through limited breakdown voltages of the control and gold-doped devices were 102 and 104 V.

The dark capacitance and depletion layer width versus reverse bias are plotted in Fig. 3 where the diffusion voltage V_D is taken to be 0.7 V. The depletion width does not saturate completely owing to some out-diffusion of the $n+$ substrate into the n region during the epitaxial film growth and device fabrication. Figure 3 also shows that the frequency dependence of the capacitance of the gold-doped units disappears when the reverse-bias voltage exceeds 6 V, an expected result when the depletion region reaches through to the $nn+$ boundary from the $p+n$ boundary.

Differential capacitance-voltage measurements were taken on the control device to probe the doping profile of the middle n region. The results show that the middle region is approximately 3 μ wide and can be completely depleted of carriers with 10-V reverse bias. Thus, the model used in the theory in Sec. II is satisfied when the reverse bias exceeds 10 V.

The dark reverse current of the junction as a function of the gate voltage is presented in Fig. 4 for various junction bias voltages at room temperature. The sharp current increase as the gate voltage increases to a certain value is due to the avalanche multiplication and breakdown at the curved edge of the junction. In the flat portion of the curves in Fig. 4, the dark reverse current is essentially independent of the gate voltage since the surface current is negligible and the depleted volume for thermal generation of dark current at the gold centers remains constant. The reverse current in the gold-doped units was approximately 1000 times higher than that of the control units.

From the data in Fig. 4, it was decided to perform all the impurity photocurrent measurements with the gate voltage set at -80 V to minimize surface leakage and breakdown. As a check, photocurrent measurements were taken with the gate voltage varied between -10 and -110 V. The turn-on time constant τ_{on} varied by about 11% while the turn-off time constant τ_{off} remained constant. The magnitude of the photocurrent varied by only 4%.

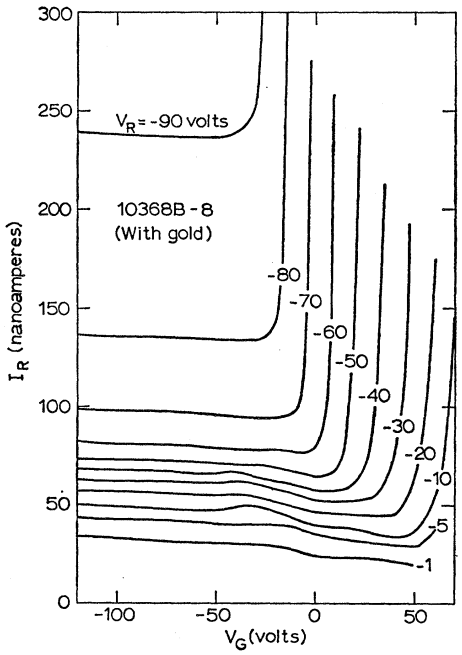

FIG. 4. Dark junction leakage current I_R as a function of the gate voltage with the junction voltage V_R as a parameter at room temperature.

IV. EXPERIMENTAL RESULTS AND DISCUSSIONS

A. Thermal-Emission Rate

The observed photocurrent waveforms of the gold-doped samples under wide range of temperature and electric field were in excellent agreement with the theoretical predictions as illustrated in Fig. 5(a). The slow transients in both the turn-on and turn-off phases were pure exponentials as evident in the semilog plot in Fig. 5(b). Deviation from exponential behavior did occur when the electric field was so large to cause avalanching as verified by dark current multiplication measurements. However, for data presented, the electric field was sufficiently low to avoid avalanche multiplication.

The control samples (without gold) were checked for photoresponse and none was observed over the range of 1.8 to 3.2 μ using a germanium filter. A very small photocurrent was recorded in the range of 1.4 to 1.9 μ using a silicon filter. The magnitude of this photocurrent was at least 100 times smaller than that from the gold-doped samples for the same experimental conditions. The control samples were also checked for deep-level impurities by a low-temperature dark capacitance technique and found to contain less than 10^{12} electrically active impurities per cm^3.

The two thermal and two optical emission rates were deduced from the data of τ_{on}, τ_{off}, Δ, and S using the results of Sec. II. The data for the optical emission rates provide some insight into the sign ambiguity discussed in Sec. II, following (9). When the two sets of photoionization cross sections are plotted versus photon energy, one of the cross sections tends towards 0.54 eV near the threshold and the other to 0.60 eV as indicated in a later figure (Fig. 12). Since the thermal activation energy of the acceptor level, from Hall and conductivity data, is 0.54 eV,[5] it is reasonable to assume that the computed cross section whose threshold is 0.54 eV is that for photoionization of electrons from the gold acceptor center, σ_n^0. The ambiguity is then resolved and the thermal-emission rates may be determined using the positive sign in (8). It is found that $e_n{}^t \gg e_p{}^t$. The assumption made by Reddi and Sah in an earlier work of gold-doped silicon diode is consistent with this result.[6]

[5] C. B. Collins, R. O. Carlson, and C. J. Gallagher, Phys. Rev. **105**, 1168 (1957).

[6] C. T. Sah and V. G. K. Reddi, Trans. IEEE **ED-11**, 345 (1964).

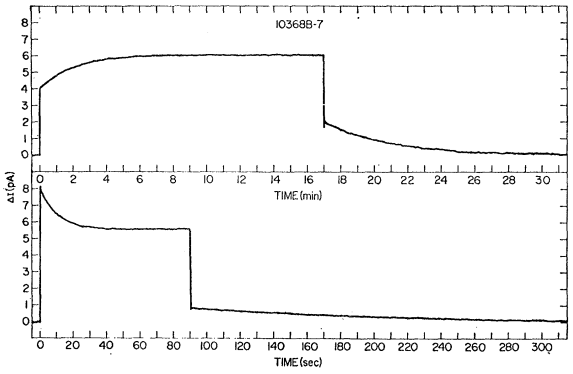

(a)

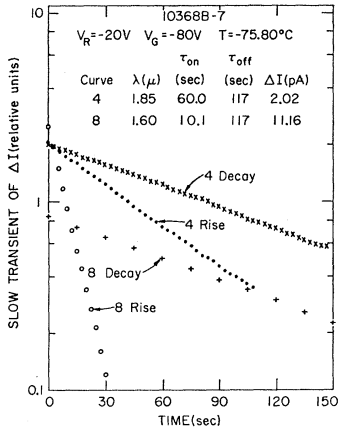

(b)

FIG. 5. Observed photocurrent. (a) Recorder trace and (b) replotted to show true exponential decay.

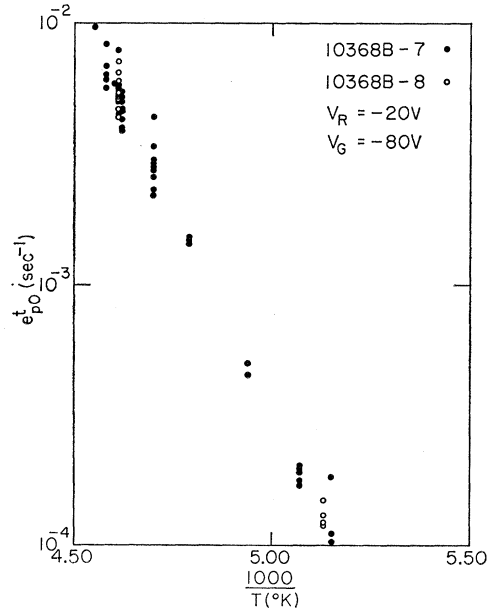

FIG. 6. Thermal-emission rate of hole, $e_p{}^t$, versus $1/T$ for two gold-doped units at different photon energies and light intensities, using Eq. (10).

It is also in agreement with the results of Senechal and Basinski[7] and more recent capacitance studies by Forbes and Sah[8] who concluded that the gold centers in the depletion region of a silicon p-n junction are probably predominantly in the neutral charge state which corresponds to $e_n{}^t \gg e_p{}^t$.

Since $e_n{}^t$ is much larger than $e_p{}^t$, the values of $e_p{}^t$ determined by an analysis of the data of τ_{on}, τ_{off}, Δ, and S are not very reliable. Thus, an alternative approach was used to calculate $e_p{}^t$ from experimental data. This involves the use of the experimentally measured dark current I_R and photocurrent ΔI (see Fig. 1), giving

$$e_p{}^0/e_p{}^t=[1+(A_J\Delta I/A_{JL}I_R)](\tau_{off}/\tau_{on})/[1+(e_n{}^0/e_n{}^t)]-1, \quad (10)$$

where A_{JL} is the junction area accessible to incident light and A_J is the total junction area. $e_p{}^t$ thus obtained from 84 measurements of dark and photocurrents at different photon energies, sample temperatures and light intensities for two diodes are plotted in Fig. 6.

From $e_p{}^t$ just obtained and $e_n{}^t+e_p{}^t$ obtained from (4), the gold concentration N_{TT} may be obtained from the measured dark leakage current using

$$I_R=qA_JW\tau_{off}e_n{}^te_p{}^tN_{TT} \quad (11)$$

$$\simeq qA_JWe_p{}^tN_{TT} \quad \text{for} \quad e_n{}^t \gg e_p{}^t. \quad (12)$$

The computed results of N_{TT} for all 84 data points are shown in Fig. 7, giving the most probable value of $N_{TT}=3.35\times10^{15}$ cm^{-3}. Using this value of N_{TT}, $e_p{}^t$ is then recomputed from the measured dark leakage current and $e_n{}^t$ from τ_{off}. These are shown in Fig. 8.

Noting that

$$e_n{}^t=c_n{}^tg_{An}N_C\exp[-(E_C-E_{Au-})/k_BT], \quad (13)$$

where

$$c_n{}^t=\sigma_n{}^t\theta_n, \quad \theta_n=(8k_BT/\pi m_N)^{1/2},$$
$$N_C=2(2k_BTm_N/\hbar^2)^{3/2},$$

the data in Fig. 8 were fitted to the equation

$$e^t=A(T/300°\text{K})^2\exp(-E_A/k_BT)$$

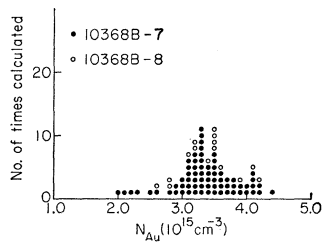

FIG. 7. Distribution of the calculated gold concentration, N_{TT}, in the depletion region from the 84 data points of Fig. 6.

[7] R. R. Senechal and J. Basinski, J. Appl. Phys. **39**, 3723 (1968).
[8] L. Forbes and C. T. Sah, Trans. IEEE **ED-16**, 1036 (1969).

with the following results:

$$\begin{aligned} e_n{}^t&: A=(1.61\pm0.12)\times10^{12}\ \text{sec}^{-1},\\ &E_A=545.48\pm1.36\ \text{meV};\\ e_p{}^t&: A=(4.80\pm0.34)\times10^{11}\ \text{sec}^{-1},\\ &E_A=588.15\pm1.33\ \text{meV}. \end{aligned} \tag{14}$$

The numerical analysis was made by a least-squares fit, and the deviation given in (14) was based on a 70% fiducial limit where the numerical constant in the Student's t distribution is about 1.07. The activation energy for $e_n{}^t$ is consistent with that from Hall measurements.[5]

B. Electric Field Dependence of Thermal-Emission Rates

The electric field dependences of the thermal-emission rates were observed at various reverse bias voltages. These are shown in Figs. 9(a) and 9(b) for various temperatures where the field was taken as the average field, $\epsilon=V_R/W$. In the range of electric field shown, there was no impact ionization as indicated by multiplication measurements.

The electric field dependences can be explained qualitatively by the Poole-Frenkel effect[9] (field-enhanced thermal ionization). In an electric field, the impurity potential barrier is lowered by some amount ΔE resulting in an increase of the emission rate given by

$$e^t(\epsilon)=e^t(0)\ \exp[\Delta E/k_BT], \tag{15}$$

which predicts a stronger field dependence at lower temperatures which is substantiated by the experimental data shown in Figs. 9(a) and 9(b).

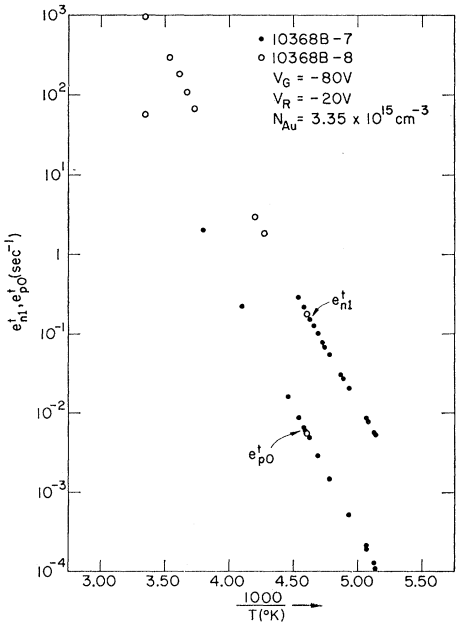

FIG. 8. Calculated thermal emission rates of electrons and holes, $e_n{}^t$ and $e_p{}^t$, using a gold concentration of $N_{TT}=3.35\times10^{15}$ cm^{-3} and the data of I_R and τ_{off}.

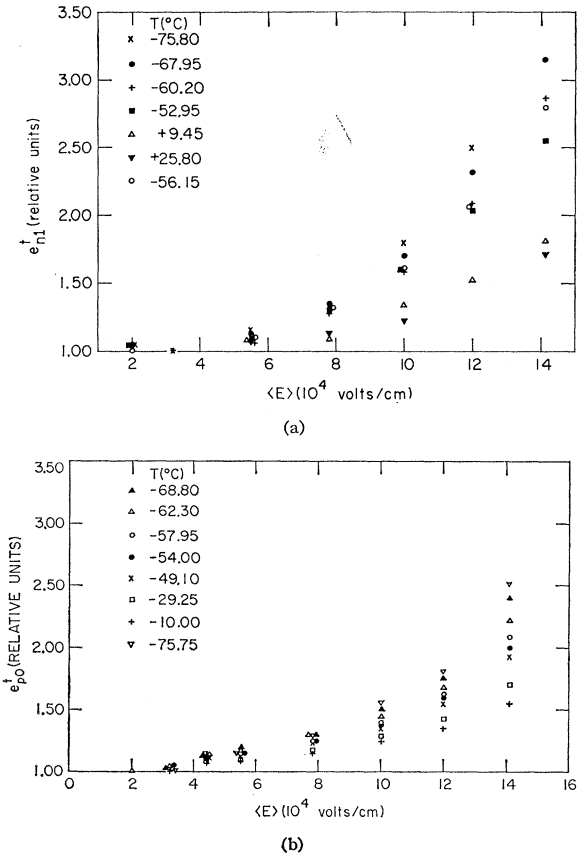

FIG. 9. Field dependence of the thermal-emission rate plotted as a function of the average electric field, $\langle E\rangle=V_R/W$. (a) $e_n{}^t$ and (b) $e_p{}^t$ for the gold acceptor level in silicon at a range of junction temperatures.

Hartke[10] has treated the Poole-Frenkel effect using a three-dimensional model and calculated the electric field dependence of the thermal emission rate for a Coulomb barrier. This is extended here to a polarization potential due to the polarization of a neutral gold atom by an electron or a hole. Lax[11] accounted for the magnitude and temperature dependences of the capture cross sections of electrons and holes by a neutral impurity center using a polarization potential of the form

$$V(r)=-A/r^4, \tag{16}$$

where $A=e^2\alpha/2K^2$ and α is the polarizability of the neutral atom, and K is the dielectric constant of silicon. For a neutral gold atom in Si, Lax estimated A to be 2×10^{-31} eV cm^4. The calculated field dependences of both the Coulomb and the polarization potential barriers are compared with the experimental results in Figs. 10(a) and 10(b) at $T=200$°K. It is evident that the theoretical Coulomb barrier predicts a much larger effect

[9] J. Frenkel, Tech. Phys. USSR **5**, 685 (1938); Phys. Rev. **54**, 647 (1938).

[10] J. L. Hartke, J. Appl. Phys. **39**, 4871 (1968).

[11] M. Lax, Phys. Rev. **119**, 1502 (1960).

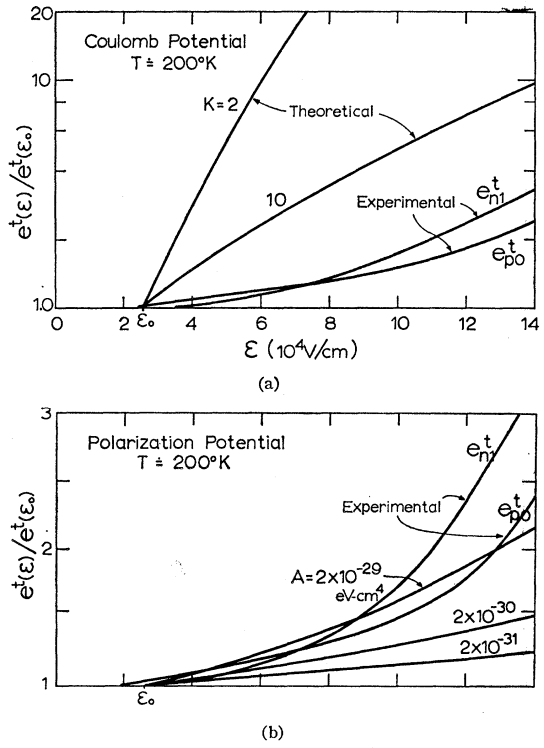

FIG. 10. Comparison of the observed field dependences of the thermal-emission rates at 200°K from Fig. 9 with the three-dimensional Poole-Frenkel theory. Upper (a) Coulombic potential, and lower (b) polarization potential.

then observed using any dielectric screening or K. The disparity is reasonable for $e_n{}^t$ where the barrier is neutral but unexpected for $e_p{}^t$ whose barrier is Coulombic.

The agreement of the data with the polarization potential model is much better as indicated in Fig. 10(b), but the required polarization constant A is about 100 times that suggested by Lax. This large difference may be partly accounted for by a smaller dielectric screening due to tight binding of the bound state. It has been shown by Sah *et al.* that the observed field dependences can be accounted for by taking into account the excited states properly.

C. Equilibrium Capture-Cross-Section Determination

Figures 9(a) and 9(b) indicate that the field dependences become negligible at 1 to 2×10^4 V/cm. Taking this as the thermal equilibrium value, then detailed balance can be used to get $\sigma_n{}^t$ using (13) and $\sigma_p{}^t$ from

$$e_p{}^t = g_{Ap}{}^{-1}\sigma_p{}^t\theta_p N_V \exp[-(E_{Au-}-E_V)/k_BT]. \quad (17)$$

Using $E_{Au-}=E_C-0.54=E_V+E_G(T)-0.54$ eV, where $E_G(T)=1.193-2.42\times10^{-4}T$ (in the range of 200 to 300°K) is obtained from a fit to the optical absorption data of Macfarlane *et al.*,[12] the capture cross sections are calculated as a function of temperature and shown in Figs. 11(a) and 11(b). The data of Bemski[13] and of Fairfield and Gokhale[14] shown in these figures for comparison do not include the degeneracy factors g_{An} and

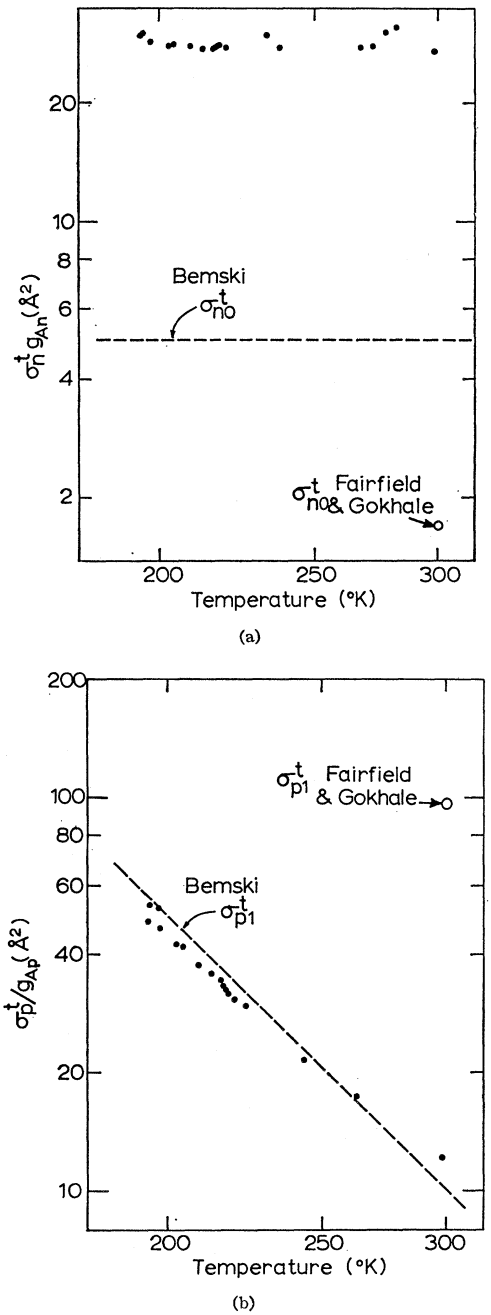

FIG. 11. Temperature dependences of the nearly equilibrium thermal-capture cross section computed from the low-field thermal-emission rates. (a) Electron and (b) hole-capture cross sections at gold acceptor center.

[12] G. G. Macfarlane, T. P. MacLean, J. E. Quarrington, and V. Roberts, Phys. Rev. **111**, 1245 (1958).

[13] G. Bemski, Phys. Rev. **111**, 1515 (1958).

[14] J. M. Fairfield and B. V. Gokhale, Solid State Electron. **8**, 685 (1965).

g_{Ap} since they were directly obtained from capture rate measurements. The agreement of our data with Bemski's data on temperature dependences exceeds the uncertainty of the energy level assumed. However, since $\sigma_n{}^t$ corresponds to electron capture by a neutral center, its temperature dependence is expected to be small.[11] Thus, the assumed value $E_{\mathrm{Au}-}=E_C-0.54$ eV is at least consistent with the observed thermal activation energy of $e_n{}^t$ (0.545 eV) given by (14). The T^{-4} temperature dependence of the hole-capture cross section by an attractive Coulombic barrier, $\sigma_p{}^t$, shown in Fig. 11(b) is also consistent with that predicted.[11]

If the emission-rate data obtained here are compared with the capture-rate data, an effective degeneracy factor can be obtained for each band. Taking the data of Fairfield and Gokhale[14] which are probably more reliable than those of Bemski since they are obtained from small signal photoconductivity measurements, then $g_{Ap}\simeq 7.5$ and $g_{An}\simeq 15$. These are not inconsistent with the degeneracy factor of the one-band model, $g_{Ap}=6$ (3 valence bands and 2 spin degeneracies) and $g_{An}=12$ (6 conduction band valleys and 2 spin degeneracies), since the data include the unknown temperature coefficients of $E_{\mathrm{Au}-}$.

D. Photoionization Cross Sections

The spectral dependences of the photoionization cross sections, $\sigma_n{}^0$ and $\sigma_p{}^0$, are presented in Fig. 12. The range was limited to below about 0.85 eV. Above this energy, the gold donor level, $E_C-E_{\mathrm{Au}+}=0.77$ eV, becomes optically active and the more complicated and less straightforward two-level photocurrent kinetics must be used, giving considerable uncertainty.

Lucovsky[15] has calculated the ground-state photoionization cross section for a deep-level impurity in semiconductors, using a δ-function potential to match the ground-state binding energy. The long-range Coulomb force is neglected. This approach seems to agree well with the experimental photoionization cross section of indium in silicon.[16] The theoretical expression is

$$\sigma_i{}^0(\hbar\omega)=(\epsilon_{\mathrm{eff}}/\epsilon_0)^2(16\pi e^2\hbar/3m^*nc)\times[E_i{}^{1/2}(\hbar\omega-E_i)^{3/2}/(\hbar\omega)^3], \quad (18)$$

where n is the index of refraction, m^* is the effective mass of the bound electron or hole, and E_i is the impurity ionization energy. $\epsilon_{\mathrm{eff}}/\epsilon_0$ is the effective field ratio which takes into account the departure of the local field at the impurity center from the macroscopic electromagnetic field in the crystal.[17]

TABLE I. Acceptor levels and effective field ratios in silicon.

Impurity	E_i (meV)	$\epsilon_{\mathrm{eff}}/\epsilon_0$	Reference
B	44	1.4	18
Al	68	2.3	18
Ga	72	2.3	18
In	155	2.5	15
In	155	3.3	18
Au	620	2.5 to 4	This work

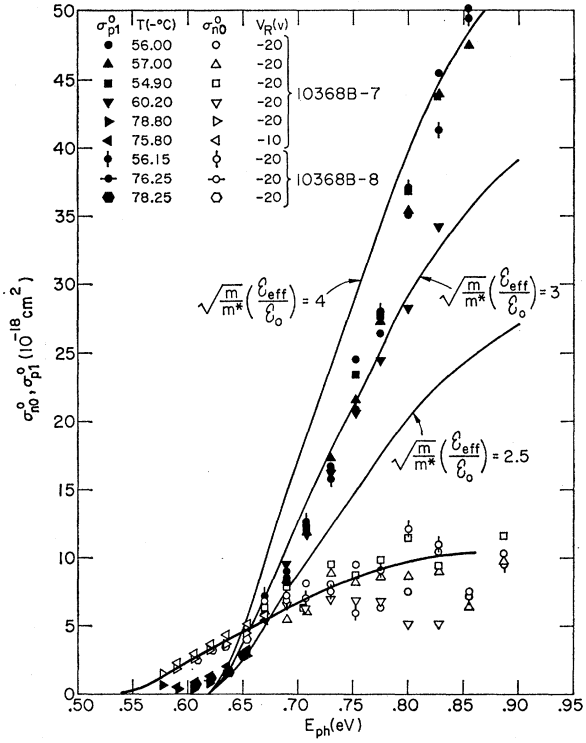

FIG. 12. Measured and theoretical (δ-function impurity-potential model) photoionization cross section as a function of photon energy.

The theory is computed and plotted in Fig. 12 for three different values of the parameter $(m/m^*)^{1/2}(\epsilon_{\mathrm{eff}}/\epsilon_0)$. Good agreement is obtained for a value of 3–4 for this parameter. If the effective mass of the hole is assumed to lie in the range of 0.5 to 1.0 m, then an effective field ratio of 2.5 to 4 is obtained. This is consistent with the trend of the data obtained for shallower acceptor levels in silicon,[15,18] which are listed in Table I.

Blakemore[19] has applied the detailed balance condition to obtain a relationship between the photoionization cross section and the radiative-capture cross section for transitions between the impurity ground state and the conduction- or valence-band states. The mean or thermally averaged radiative-capture cross section is given by

$$\bar{\sigma}_r{}^0=[gn^2/2c^2m^*(k_BT)^2]\times\int_0^\infty (E_i+E)^2\sigma_i{}^0(\hbar\omega)e^{-E/k_BT}dE, \quad (19)$$

[15] G. Lucovsky, Solid State Commun. **3**, 299 (1965).
[16] R. Newman, Phys. Rev. **99**, 465 (1955).
[17] D. L. Dexter, in *Solid State Physics*, edited by F. Seitz and D. Turnbull (Academic Press Inc., New York, 1958), Vol. 6.
[18] H. B. Bebb and R. A. Chapman, J. Phys. Chem. Solids **28**, 2087 (1967).
[19] J. S. Blakemore, Phys. Rev. **163**, 809 (1967).

where E is the carrier kinetic energy measured from the band edge and g is the degeneracy factor.

The radiative-capture cross section of holes by a negatively charged gold acceptor center can then be obtained from (19) using (18). Using a numerical value of $(m/m^*)^{1/2}(\epsilon_{\text{eff}}/\epsilon_0)=3.5$ and a degeneracy of the ground state of $g=6$, then

$$\bar{\sigma}_{rp}{}^0=6.3\times10^{-21}(T/300°\text{K})^{1/2}\ \text{cm}^2.$$

The optical cross-section data for electron emission, $\sigma_n{}^0$, are also fitted with the δ-function potential giving an effective field ratio of $(m/m^*)^{1/2}(\epsilon_{\text{eff}}/\epsilon_0)\simeq1$. The mean radiative-capture cross section of electrons can be estimated from this result using the procedure just described, giving a value about $\frac{2}{3}$ that of $\bar{\sigma}_{rp}{}^0$ given above, if a ground-state degeneracy of $g=12$ is assumed. The extrapolated electron photoionization threshold is approximately 0.54 eV as indicated in Fig. 12, which is consistent with the thermal activation energy of the electron emission rate $e_n{}^t$ obtained from Fig. 8.

The field dependences of the photoionization cross section were also investigated. The results in the range of $3\text{–}15\times10^4$ V/cm show essentially no field dependence with a random error of about $\pm10\%$ at 1.65 and 1.8 μ and in the range of -53 to -76°C.

ACKNOWLEDGMENTS

The authors would like to thank L. L. Rosier and L. Forbes for numerous discussions. The numerical fits of the data in Fig. 8 were made by A. B. Tole. W. W. Chan performed many numerical data analyses and helped in the preparation of the manuscript. The epitaxial silicon slices were provided by R. N. Tucker of Fairchild Semiconductor Laboratory. We would also like to thank the other members of the Solid State Electronics Laboratory who had helped in setting up the silicon-device fabriaction facilities and electrical and optical measurement apparatus.

APPENDIX

The recombination statistics for multilevel impurities, which have been treated in detail by Sah and Shockley,[20] can be applied to the two levels of gold in silicon. In the depletion region of a reverse-biased junction ($n,p\simeq0$), the concentrations of the different charge states of the gold atoms are given by

$$N_0=N_{TT}/(1+\alpha+\beta),\qquad\text{(A1)}$$

$$N_1=\alpha N_0,\qquad\text{(A2)}$$

$$N_{-1}=\beta N_0,\qquad\text{(A3)}$$

where $\alpha=e_{p0}{}^t/e_{n1}{}^t$ and $\beta=e_{n0}{}^t/e_{p-1}{}^t$. N_0, N_1, N_{-1} are the concentrations of neutral, negatively ionized, and positively ionized gold atoms. The subscript denotes whether or not the gold atom has trapped an extra electron or has given up an electron to the host lattice. That is, -1 indicates that the center is positively ionized (less one electron), while 1 denotes that the center is negatively ionized (one extra electron). Of course, 0 implies that the gold center is neutral with respect to the lattice. Because a multilevel impurity is being considered, it is necessary to attach an additional subscript $(-1, 0, 1)$ to the emission rates to denote the charge state of the gold center just prior to emission of the electron or hole. The thermal and optical emission rates $e_n{}^t$, $e_p{}^t$, $e_n{}^0$, and $e_p{}^0$ that were considered in the text become $e_{n1}{}^t$, $e_{p0}{}^t$, $e_{n1}{}^0$, and $e_{p0}{}^0$ in this notation.

The four thermal emission rates can be estimated from the capture cross-section data of Bemski,[13] and Fairfield and Gokhale[14] with the result that the hole-emission rate from positively ionized gold centers, $e_{p-1}{}^t$, is much larger than $e_{n0}{}^t$, the thermal emission rate of electrons from neutral gold atoms; also, $\beta\ll\alpha$. Thus the concentration of positively ionized gold centers is several orders of magnitude below the concentration of neutral and negatively ionized centers.

When light is incident on the depletion region, Eqs. (A1)–(A3) are still applicable except that now

$$\alpha=\frac{e_{p0}{}^t+e_{p0}{}^0}{e_{n1}{}^t+e_{n1}{}^0}\quad\text{and}\quad\beta=\frac{e_{n0}{}^t+e_{n0}{}^0}{e_{p-1}{}^t+e_{p-1}{}^0},$$

where $e_{p0}{}^0$, $e_{n1}{}^0$, $e_{n0}{}^0$, and $e_{p-1}{}^0$ are the optical emission rates due to the photoexcitation of the electrons and holes. Their values depend on the photon energy and intensity. The condition $\beta\ll\alpha$ still holds as long as $e_{n0}{}^0$ remains small relative to $e_{n0}{}^t$. That is, the number of positively ionized gold centers will remain negligible provided the photon energy is not great enough to photoexcite an appreciable number of electrons from neutral gold atoms, thereby greatly increasing the number of positively ionized gold atoms. The threshold energy for this condition is about 0.8 eV so that the single-level approximation should be very good for $\hbar\omega<0.8$ eV. However, the single-level approximation is probably valid for photon energies up to 0.85 or 0.90 eV since it is usually necessary to go above the threshold energy to obtain appreciable photoexcitation.

The analysis of the impurity photocurrent effect can be performed with the donor level of gold included (two-level case). The expression for the photocurrent when the light is turned on is found to be

$$j(t)/qW=Q_+e^{-t/\tau_+}+Q_-e^{-t/\tau_-}+Q_3.\qquad\text{(A4)}$$

The constants are defined below:

$$\tau_\pm{}^{-1}=\tfrac{1}{2}(a_1+a_2+a_3+a_4)\pm[\tfrac{1}{2}(a_1+a_2+a_3+a_4)^2-(a_1a_4+a_2a_3+a_3a_4)]^{1/2},$$

$$Q_\pm=\frac{\pm(e_1+e_2\alpha_\pm)}{\tau_+{}^{-1}-\tau_-{}^{-1}}\times[a_4N_{10}-a_2N_{00}+\tau_\mp{}^{-1}(N_{1F}-N_{10})],$$

[20] C. T. Sah and W. Shockley, Phys. Rev. **109**, 1103 (1958).

$$Q_3=\tfrac{1}{2}[a_4N_{-1F}+(a_1+a_2)N_{0F}+a_3N_{-1F}],$$

$$\alpha_\pm=(a_4-\tau_\pm^{-1})/a_2,$$

$$e_1=a_4-a_3,$$

$$e_2=a_1+a_2-a_3,$$

$$N_{0F}=\frac{N_{TT}}{1+a_2/a_4+a_1/a_3},\quad N_{1F}=\frac{a_2}{a_4}N_{0F},$$

$$N_{-1F}=\frac{a_1}{a_3}N_{0F},$$

$$a_1=e_{n0}{}^t+e_{n0}{}^0,\quad a_2=e_{p0}{}^t+e_{p0}{}^0,$$

$$a_3=e_{p-1}{}^t+e_{p-1}{}^0,\quad a_4=e_{n1}{}^t+e_{n1}{}^0,$$

$$N_{00}=\frac{N_{TT}}{1+e_{p0}{}^t/e_{n1}{}^t+e_{n0}{}^t/e_{p-1}{}^t},\quad N_{10}=\frac{e_{p0}{}^t}{e_{n1}{}^t}N_{00},$$

$$N_{-10}=\frac{e_{n0}{}^t}{e_{p-1}{}^t}N_{00}.$$

Again, the values of the four optical emission rates depend on the energy and intensity of the incident photons. If the incident photon energy is assumed to be less than 0.8 eV so that $e_{n0}{}^0\simeq 0$, and if use is made of the fact that $e_{p-1}{}^t\gg e_{n1}{}^t$, $e_{n0}{}^t$, $e_{p0}{}^t$, Eq. (A4) reduces to Eq. (2) in the text.

PHYSICAL REVIEW B VOLUME 1, NUMBER 2 15 JANUARY 1970

Effects of Heat Treatment and Background Divalent Cation Impurity on the Growth of *F* Centers in Highly Pure KCl Crystals

P. C. MEHENDRU

Solid State Physics Division, National Physical Laboratory, New Delhi 12, India

(Received 10 December 1968; revised manuscript received 26 September 1969)

The effects of heat treatment and background divalent cation impurity on the growth of *F* centers in highly pure KCl crystals (divalent impurity concentration $\lesssim 1$ ppm) have been studied from the growth of the thermoluminescence peaks. For a heating rate of 40°C/min, these peaks occur at 135 and 190°C (for highly pure crystals) and at 95, 135, and 190°C (for crystals containing ~ 30 ppm of background divalent cation impurity). The peaks at 95, 135, and 190°C are associated with the *F* centers due to the background divalent cation impurities, and with the first- and the second-stage *F* centers, respectively. The growth of the thermoluminescence areas with the time of x irradiation can be fitted with the equations of Mitchell, Wiegand, and Smoluchowski and of Frohlich. Various parameters in these equations are evaluated and discussed.

I. INTRODUCTION

IN highly pure KCl crystals, x irradiated at room temperature (RT), only two thermoluminescence peaks are observed.[1] The two peaks occur at 135 and 190°C, when the heating rate is 40°C/min. The rates of increase of areas Δ_i and Δ_g under the 135 and the 190°C thermoluminescence peaks, respectively, are given by

$$\Delta_i=Kn(1-e^{-bt}) \tag{1}$$

and

$$\Delta_g=K[at-(a/c-n')(1-e^{-ct})], \tag{2}$$

where n and n' are the concentrations of the anion vacancies released into the crystal by some radiochemical processes perhaps involving some impurity or impurity-defect complex and which give rise to the first and the second stage of *F* centers' coloration, respectively; b and c are the rates of capture of electrons by n and n' vacancies, respectively; a is the rate of generation of the anion vacancies by the x rays, and K is the ratio of the total thermoluminescence area $\Delta(=\Delta_i+\Delta_g)$ to the OD_F (the optical density at the peak of *F* band) or to the total number f of *F* centers formed by the x irradiation.

It was shown earlier[1] that the concentrations[2-4] f_i and f_g corresponding to the first- and the second-stage *F* centers, respectively, are related to the thermoluminescence areas Δ_i and Δ_g by the relation

$$\frac{\Delta_i}{f_i}=\frac{\Delta_g}{f_g}=\frac{\Delta}{f}=K. \tag{3}$$

This result is rather important, since it shows that the areas under the 135 and 190°C thermoluminescence peaks in highly pure KCl crystals are separately related

[1] S. C. Jain and P. C. Mehendru, Phys. Rev. **140**, A957 (1965).

[2] The total concentration f of *F* centers was separated into the concentrations f_i and f_g by the method of Mitchell *et al.* (see Ref. 3), and of Fröhlich (see Ref. 4). Although the significance of the parameters in the equations of Mitchell *et al.* is far from well established, it is a convenient method for separating the total concentration f into the concentrations f_i and f_g.

[3] P. V. Mitchell, D. A. Wiegand, and R. Smoluchowski, Phys. Rev. **121**, 484 (1961).

[4] F. Fröhlich, Z. Naturforsch. **16a**, 211 (1961); **17a**, 327 (1962).